DETC2005-85368

MODELLING OF MAGNETIC PULL IN LARGE SIZE GENERATOR

Paolo Pennacchi
Dipartimento di Meccanica
Politecnico di Milano
Via La Masa 34
I-20156 Milano
paolo.pennacchi@polimi.it

Lucia Frosini
Dipartimento di Ingegneria Elettrica
Università degli studi di Pavia
Via Ferrata 1
I-27100 Pavia
lucia@unipv.it

ABSTRACT

This paper presents a method to analyze the dynamical behaviour of large size generators due to the magnetic pull. In rotating electrical machines, the electromagnetic radial forces acting upon rotor and stator surfaces are very large, but they are balanced when the rotor is concentric with the stator. Similarly, the tangential forces produce only an axially rotating moment. If the rotor becomes eccentric, then an imbalance of these forces occurs, so that a net radial electromagnetic force, known as Unbalanced Magnetic Pull (UMP), is developed. The models traditionally proposed in the literature to study the UMP can be considered as reliable in case of small size electrical machines supported by rolling bearings. On the contrary, in case of large size machines, such as turbo-generators supported by oil-film bearings, the approximation of circular orbits of the rotor is not acceptable. Nevertheless, the authors who have dealt with UMP in big size generators have disregarded that these rotor filtered orbits are elliptical and generally the orbit centres are not concentric with the stator.

In order to provide a more realistic model and an original contribution, in this work the actual distribution of the air-gap length during the rotation will be determined in analytical terms, by taking into account the effects produced by the actual rotor orbit. The actual UMP is calculated by using the air-gap permeance approach and the simulation of the dynamical behaviour of a 320 MW generator is presented, showing the harmonic content of the UMP and the presence of non-linearities.

Keywords: Unbalanced magnetic pull, generator, rotor dynamics, non-linearity.

INTRODUCTION

Rotor eccentricity can occur in rotating electrical machines, as a consequence of different causes (errors during assembly, bearings wear, bow of the shaft, etc.) or of the normal operating of a flexible machine. In rotating electrical machines, the electromagnetic radial forces acting upon rotor and stator surfaces are very large, but they are balanced when the rotor is concentric with the stator. Similarly, the tangential forces produce only an axially rotating moment.

If the rotor becomes eccentric, then an imbalance of these forces occurs, so that a net radial force is developed. This radial force, known as Unbalanced Magnetic Pull (UMP), causes vibrations and noise emission, speeds up the bearing wear and can even produce a rub between rotor and stator with a consequent damage of the windings.

Many researches have been addressed to this field since the 60's, by developing specific problems or applications.

The works available in literature can be distinguished according to:
- the type of eccentricity (static or dynamic),
- the type of machine (induction, synchronous, brushless),
- the type of studied effect (calculation of UMP, definition of fault indicators, modelling the dynamic behaviour of the machine).

The majority of the works in literature take into consideration the induction motors, mainly for two reasons:
- they are the most spread in industry (from small to large power);
- their air-gaps are smaller than other machines (0.3-3 mm).

Recent works have been addressed to the study of eccentricity in:
- synchronous machines, which are normally used as generators of large power and can be with salient poles ("squat" rotor, small air-gap: 10-15 mm) or smooth rotor ("slim" rotor, large air-gap: 30-100 mm);
- brushless motors with permanent magnets, which are used for small power in automation and robotics (small air-gap: 0.5 mm).

In this paper, the UMP in smooth generators is analyzed. Few papers are present in literature about these topics. In [1] a study is presented in which, despite of the fact that a 500 MW, 3000 rpm generator is analyzed, rotor orbits are considered as circular. This can be a first approximation, since such kind of large machines are supported by oil-film bearings, whose anisotropy can hardly determine circular orbits. Anyhow, the model presented shows that the resulting UMP has a constant component and a 2X harmonic component only.

In [2] some results presented in [3] for induction motors are used and also a simplified model with isotropic bearings (thus circular orbits) and a Jeffcott rotor is presented. The approximate expression of the air-gap allows the authors to express the UMP in analytic closed form for different pole-pairs. Also in this case, for one pole-pair generator, the UMP has a constant component and a 2X harmonic component only. In [4] the results of [2] are used to study the stability of a 70MW hydro-generator, but the authors uses a very simplified Euler-Bernoulli beam for the entire rotor.

The model presented in this paper introduces instead a very accurate calculation of the air-gap distribution depending on the position in a general time instant of the rotor inside the stator. The UMP, which is calculated by means of the air-gap permeance approach, is then function of both time and position. The method is applied to a model of a 320 MW, 3000 rpm 3-phase generator, which is modelled by means of standard finite beam elements normally used in rotor dynamics. The UMP is calculated for all the elements of the generator model that corresponds to the slotted part. The Newmark method is used to integrate the non linear dynamic equations of the system. The obtained results confirm the presence of the static and 2X harmonic component force but show the presence of a 1X component and of non-linear effects too.

UMP MODELLING

Traditional models about UMP, which deal with the problem under an electrical point of view, normally present the distinction between static eccentricity and dynamic eccentricity. Using the electrical terminology, in the first case, the position of minimum radial length of the air-gap is fixed in the space: the rotor is symmetrical with respect to its axis and rotates about it. In the second case, the position of minimum radial length of the air-gap rotates with the rotor: in case of a machine, which can be considered as rigid, the shaft axis does not coincide with the rotor axis (the rotor does not rotate about its axis).

The difference among static and dynamic eccentricity is actually relevant in case of electric motors of small to medium size in which very stiff bearing, normally rolling bearing, are used. The greater part of the available literature about UMP refers to these electric machines [3] [5] [6] [7], in which very often the rotor is squat and can be considered as rigid or operates in any case below its first critical speed. Some other studies about generators [1] [2] present the same distinction that however is not so appropriate for high-speed generators of turbo-generators: first, these machines operate over their first critical speed, therefore are flexible and present always the so called dynamic eccentricity; second, since oil-film bearing are used, the oil-film forces determine the rotor centreline to describe a path during the run-up, therefore the rotor centreline

is not statically concentric to the stator, unless a specific alignment operation is performed.

Since this paper deals with high-speed generators of turbo-generators, we do not consider the distinction between statical and dynamical eccentricity and the air-gap distribution is determined in the general case as a function of the position of the rotor in a general time instant w.r.t. the stator. Moreover, the dynamical deformation of the rotor produces an air-gap distribution that is not constant along the span of the rotor. For this reason, the air-gap distribution has to be defined for each section of the machine slotted part.

Let consider figure 1 in which the relative position of the rotor and the stator are shown in a general time instant t, for a generator section, and the average air-gap is intentionally magnified for graphical clearness. The reference system $S'(x', O', y')$ is fixed and centred in the stator centre O', while the reference system $S''(x'', O'', y'')$ has its centre O'' that corresponds to the rotor centreline. Due to the presence of lateral vibrations, the rotor centre O describes an orbit around the centreline. Therefore, the eccentricity between the stator and the rotor centre is determined by two components: the offset $\overline{O'O''}$ due to the centreline path during the run-up and the lateral vibration $\overline{O''O}$ of the rotor. The position $\mathbf{x}$ of the rotor centre $P_0 \equiv O$ in a general time instant t depends on the previous time history and on the exciting systems acting on the shaft. The reference system $S(x, O, y)$ is centred in the rotor centre. Since the aim is to determine the air-gap radial distribution, the angular relative position of S and S' is not relevant and for simplicity the reference axes are considered as parallel.
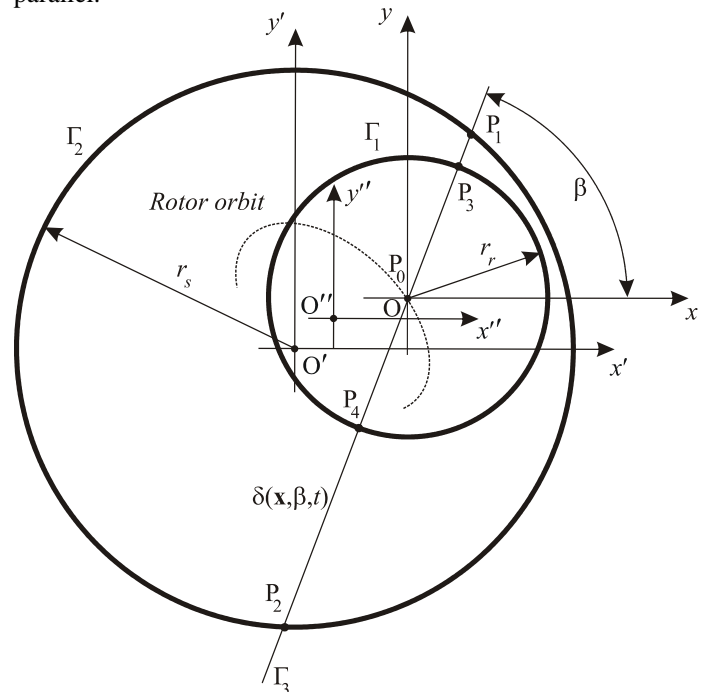

Figure 1: Calculation of the air gap $\delta\left(\mathbf{x}, \beta, t\right)$.

The equations of the stator circumference $\Gamma_2^{(S)}$ in the reference S are in parametric form:

Copyright © 2005 by ASME

$$\Gamma_2^{(S)} : \begin{cases} x(t) = x_{O'}(t) + r_s \cos\alpha \\ y(t) = y_{O'}(t) + r_s \sin\alpha \end{cases}, 0 \le \alpha < 2\pi \qquad (1)$$

and in implicit form:

$$(x - x_{O'})^2 + (y - y_{O'})^2 = r_s^2 \qquad (2)$$

in which $(x_{O'}(t), y_{O'}(t))$ are the co-ordinates of O′ in the reference system S in a general time instant t. These values are actually the absolute vibration of rotor w.r.t. the stator centre. The equation of a general line $\Gamma_3^{(S)}$ in reference system S passing through P_0 is:

$$\Gamma_3^{(S)}: \quad y = x \tan\beta, \ \left|\beta\right| \ne \frac{\pi}{2} \qquad (3)$$

$$\Gamma_3^{(S)}: \quad x = 0, \ \left|\beta\right| = \frac{\pi}{2} \qquad (4)$$

The angle β is sometimes referred as *spatial angle* in Electrical Engineering literature. If $\left|\beta\right| \ne \frac{\pi}{2}$ the intersections $\{P_1, P_2\} = \Gamma_3 \cap \Gamma_2$ between the general line passing through P_0 and the stator are obtained by replacing eq. (3) in eq. (2):

$$\{P_1, P_2\}^{(S)}: \quad \begin{cases} (x - x_{O'})^2 + (x\tan\beta - y_{O'})^2 = r_s^2, \\ y = x\tan\beta \end{cases} \ \left|\beta\right| \ne \frac{\pi}{2} \quad (5)$$

After some manipulation, first equation of eq. (5) becomes:

$$x^2 - 2x\left(x_{O'} \cos^2\beta + y_{O'} \cos\beta \sin\beta\right) - \\ -r_s^2 \cos^2\beta + x_{O'}^2 \cos^2\beta + y_{O'}^2 \cos^2\beta = 0 \qquad (6)$$

Eq. (6) is a 2nd order algebraic equation in the unknown x and has two solutions: that with $+$ sign corresponds to intersection points for $\left|\beta\right| < \frac{\pi}{2}$, like point P_1 in figure 1, while that with $-$ sign to intersection points for $-\pi < \beta < -\frac{\pi}{2} \cup \frac{\pi}{2} < \beta \le \pi$, like point P_2 in figure 1. After some simplifications, co-ordinates of points P_1 and P_2 result:

$$\{P_1, P_2\}^{(S)}:$$

$$\begin{cases} x_{P_1,P_2} = x_{O'} \cos^2\beta + y_{O'} \cos\beta \sin\beta \pm \\ \pm\sqrt{\cos^2\beta\left(r_s^2 - (y_{O'}\cos\beta - x_{O'}\sin\beta)^2\right)} \\ y_{P_1,P_2} = x_{O'} \cos\beta \sin\beta + y_{O'} \sin^2\beta \pm \\ \pm\tan\beta\sqrt{\cos^2\beta\left(r_s^2 - (y_{O'}\cos\beta - x_{O'}\sin\beta)^2\right)} \end{cases}, \qquad (7)$$

$$\left|\beta\right| \ne \frac{\pi}{2}$$

The case of $\left|\beta\right| = \frac{\pi}{2}$ is not relevant as shown in eqs. (22) and (23). The equations of the rotor circumference $\Gamma_1^{(S)}$ in the reference S are in parametric form:

$$\Gamma_1^{(S)}: \begin{cases} x = r_r \cos\gamma \\ y = r_r \sin\gamma \end{cases}, 0 \le \gamma < 2\pi \qquad (8)$$

and in implicit form:

$$x^2 + y^2 = r_r^2 \qquad (9)$$

The intersections $\{P_3, P_4\} = \Gamma_3 \cap \Gamma_1$ between the general line passing through P_0 and the rotor are given replacing eq. (3) in eq. (9):

$$\{P_3, P_4\}^{(S)}: \begin{cases} x^2 + y^2 = r_r^2 \\ y = x\tan\beta \end{cases} \qquad (10)$$

After some manipulation, first equation of eq. (10) becomes:

$$x^2 - r_r^2 \cos^2\beta = 0 \qquad (11)$$

Eq. (11) has two solutions: that with $+$ sign corresponds to intersection points for $\left|\beta\right| < \frac{\pi}{2}$, like point P_3 in figure 1, while that with $-$ sign to intersection points for $-\pi < \beta < -\frac{\pi}{2} \cup \frac{\pi}{2} < \beta \le \pi$, like point P_4 in figure 1. After some simplifications, co-ordinates of points P_3 and P_4 result simply:

$$\{P_3, P_4\}^{(S)}: \begin{cases} x_{P_3,P_4} = \pm r_r^2 \cos\beta \\ y_{P_1,P_2} = \pm r_r^2 \sin\beta \end{cases} \qquad (12)$$

Again, the case of $\left|\beta\right| = \frac{\pi}{2}$ is not relevant.

3   Copyright © 2005 by ASME

Finally, the air gap $\delta(\mathbf{x}, \beta, t)$ is given by the distance between points P_1 and P_3 for $|\beta| < \dfrac{\pi}{2}$ and between points P_2 and P_4 for $-\pi < \beta < -\dfrac{\pi}{2} \cup \dfrac{\pi}{2} < \beta \leq \pi$ respectively:

$$\delta(\mathbf{x}, \beta, t) = \sqrt{\left(x_{P_1, P_2} - x_{P_3, P_4}\right)^2 + \left(y_{P_1, P_2} - y_{P_3, P_4}\right)^2} \qquad (13)$$

The closed form of the air gap $\delta(\beta, t)$, after some algebra, is:

$$\delta_{rh}(\mathbf{x}, \beta, t) = \begin{pmatrix} r_s^2 + r_r^2 + x_{O'}^2 \cos 2\beta + 4x_{O'} y_{O'} \cos\beta \sin\beta - \\ -y_{O'}^2 \cos 2\beta - 2r_r \left(x_{O'} \cos\beta + y_{O'} \sin\beta\right) + \\ +2\left(x_{O'} + y_{O'} \tan\beta - r_r \sec\beta\right) \cdot \\ \cdot\sqrt{\cos^2\beta\left(r_s^2 - \left(x_{O'} \sin\beta - y_{O'} \cos\beta\right)^2\right)} \end{pmatrix}^{1/2} \qquad (14)$$

if the spatial angle satisfies the condition $|\beta| < \dfrac{\pi}{2}$ and

$$\delta_{lt}(\mathbf{x}, \beta, t) = \begin{pmatrix} r_s^2 + r_r^2 + x_{O'}^2 \cos 2\beta + 4x_{O'} y_{O'} \cos\beta \sin\beta - \\ -y_{O'}^2 \cos 2\beta + 2r_r \left(x_{O'} \cos\beta + y_{O'} \sin\beta\right) - \\ -2\left(x_{O'} + y_{O'} \tan\beta + r_r \sec\beta\right) \cdot \\ \cdot\sqrt{\cos^2\beta\left(r_s^2 - \left(x_{O'} \sin\beta - y_{O'} \cos\beta\right)^2\right)} \end{pmatrix}^{1/2} \qquad (15)$$

if $-\pi < \beta < -\dfrac{\pi}{2} \cup \dfrac{\pi}{2} < \beta \leq \pi$.

In order to calculate the radial force due to the UMP on a general element *j*-th of the rotor, once that the spatial air-gap distribution is known w.r.t. the considered rotor element and the stator, the Maxwell stress tensor is used:

$$\sigma_r = \frac{1}{2\mu_0}\left(B_r^2 - B_\theta^2\right)$$
$$\sigma_\theta = \frac{1}{\mu_0} B_r B_\theta \qquad (16)$$

where the subscript r indicates the radial component and θ the tangential component, B is the air-gap flux density and μ_0 is the vacuum magnetic permeability. It is generally commonly accepted that the tangential component is negligible, as done in [1] [5]. This is a rather acceptable approximation only for concentric rotors. In case of eccentric rotors this is less reliable, but there are some studies, even if related to cage induction motors [8], that suggest that is reasonable to neglect the tangential stress, providing that large eccentricities are avoided. Therefore, for simplicity, it is assumed that $B_\theta = 0$.

The magnetic flux Φ_r that crosses radially the air-gap is given by:

$$\Phi_r = M \Lambda \qquad (17)$$

where M is the magnetomotive force produced by the winding currents of one pole-pair and Λ is the permeance of the magnetic circuit carrying the magnetic flux Φ_r.

Since the permeance of the air-gap is much smaller than the permeance of the iron core, the last is neglected in the calculation of the magnetomotive force M:

$$M = \frac{\Phi_r}{\Lambda} = \frac{B_r \bar{S}}{\dfrac{\mu_0 \bar{S}}{2\delta}} = \frac{2 B_r \delta}{\mu_0} \qquad (18)$$

where $\bar{S}$ is any normal surface crossed by the magnetic flux. The expression of the magnetomotive force is expanded in a Fourier series: the first harmonic component has a sinusoidal spatial distribution through the air-gap with period twice the pole pitch τ and its amplitude is sinusoidally variable during the time, depending on the supply frequency f_s:

$$M_1(z, t) = \bar{M}_1 \cos\left(\omega t - \frac{\pi z}{\tau}\right) =$$
$$= \bar{M}_1 \cos\left(\omega t - \frac{\pi z}{\dfrac{\pi R}{p_p}}\right) = \bar{M}_1 \cos\left(\omega t - p_p \frac{z}{R}\right) \qquad (19)$$

where $\omega = 2\pi f_s$, R is the mean air-gap radius, z is the distance around the air-gap from a reference point, p_p the pole-pairs and $z/R = \beta$. In fact, the mean air-gap length δ is small compared to the mean air-gap radius R, therefore $R \approx r_s \approx r_r$. By considering for simplicity only the first harmonic component of the magnetomotive force of the exciting current per each pole, the air-gap flux density becomes:

$$B_r(\mathbf{x}, \beta, t) = \mu_0 \frac{M_1(\beta, t)}{2\delta(\mathbf{x}, \beta, t)} = \mu_0 \frac{\bar{M}_1 \cos\left(\omega t - p_p \beta\right)}{2\delta(\mathbf{x}, \beta, t)} \qquad (20)$$

By using eq. (20) in eq. (16), the Maxwell stress becomes:

$$\sigma_r(\mathbf{x}, \beta, t) = \frac{B_r^2(\beta, t)}{2\mu_0} = \mu_0 \frac{M_1^2(\beta, t)}{8\delta^2(\mathbf{x}, \beta, t)} =$$
$$= \frac{\mu_0 \bar{M}_1^2}{8} \frac{\cos^2\left(\omega t - p_p \beta\right)}{\delta^2(\mathbf{x}, \beta, t)} \qquad (21)$$

4

Copyright © 2005 by ASME

The resultant forces, due to the UMP, on the considered element j-th of the rotor, in horizontal and vertical direction, are finally obtained by integrating Maxwell stress of eq. (21):

$$F_{x,UMP}^{(j)}(\mathbf{x},t) = \int_0^{2\pi} \sigma_r(\mathbf{x},\beta,t) r_r^{(j)} l^{(j)} \cos\beta d\beta =$$

$$= \frac{\mu_0 \bar{M}_1^2}{8} r_r^{(j)} l^{(j)} \left(\int_{-\pi/2}^{\pi/2} \frac{\cos\beta \cos^2(\omega t - p_p \beta)}{\delta_{rh}^2(\mathbf{x},\beta,t)} d\beta + \int_{\pi/2}^{3\pi/2} \frac{\cos\beta \cos^2(\omega t - p_p \beta)}{\delta_{lt}^2(\mathbf{x},\beta,t)} d\beta \right) \quad (22)$$

$$F_{y,UMP}^{(j)}(\mathbf{x},t) = \int_0^{2\pi} \sigma_r(\mathbf{x},\beta,t) r_r^{(j)} l^{(j)} \sin\beta d\beta =$$

$$= \frac{\mu_0 \bar{M}_1^2}{8} r_r^{(j)} l^{(j)} \left(\int_{-\pi/2}^{\pi/2} \frac{\sin\beta \cos^2(\omega t - p_p \beta)}{\delta_{rh}^2(\mathbf{x},\beta,t)} d\beta + \int_{\pi/2}^{3\pi/2} \frac{\sin\beta \cos^2(\omega t - p_p \beta)}{\delta_{lt}^2(\mathbf{x},\beta,t)} d\beta \right) \quad (23)$$

where $r_r^{(j)}$ and $l^{(j)}$ are respectively the radius and the length of the element j-th of the rotor.

APPLICATION TO A GENERATOR

In order to evaluate the dynamical effects of the UMP in rotating machinery, the method described in the previous section is applied to the model of a 320 MW smooth 3-phase generator with its exciter. For simplicity, only the generator model is considered and the turbine parts of the shaft line of the turbo-generator are omitted. The considered machine operates at 3000 rpm, the supply frequency is 50 Hz (being the machine synchronous) and has only one pole-pair. Due to its design, this type of generator presents polar stiffness asymmetry that can cause by itself 2X vibration component [9] [10] [11]. Anyhow this fact is not considered and modelled here in order not to mask the 2X vibration due to UMP.

The rotor is modelled by means of 33 beam element, with 4 d.o.f.s per node, and is supported by three oil-film bearings (figure 2). Even if the oil-film forces are not constant and depend, among other causes, on the loads on the bearings, in order to evaluate only the effects of the UMP, they are considered constant and linearized damping and stiffness coefficients are used. This simplification allows not to integrate Reynolds equation and not to introduce non-linearities that can mask possible similar effects caused by the UMP.
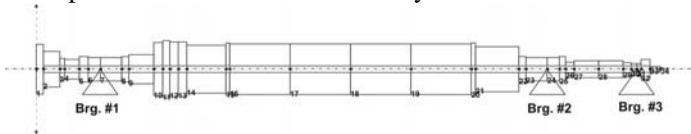

Figure 2: Generator model (mass diameters).

Bearing #1 and #2 are elliptical and equal, while bearing #3 is of tilting-pad type. The linearized coefficients employed for the simulation are calculated at the operating speed using reference [12] and are reported in table 1 (subscript x indicates horizontal direction and y vertical direction).

Table 1: Linearized dynamic coefficients for the bearings.

	k_{yy}	k_{yx}	k_{xy}	k_{xx}
Brg. #1	1.00e9	−7.00e8	1.20e8	6.00e8
Brg. #2	1.00e9	−7.00e8	1.20e8	6.00e8
Brg. #3	8.00e7	0	0	8.00e7

	r_{yy}	r_{yx}	r_{xy}	r_{xx}
Brg. #1	2.00e7	−1.00e7	−1.00e7	2.00e7
Brg. #2	2.00e7	−1.00e7	−1.00e7	2.00e7
Brg. #3	2.00e6	0	0	2.00e6

The supporting structure is modelled by means of pedestals. The fully assembled system (rotor + bearings + foundation) mass matrix, which takes also into account the secondary effect of the rotatory inertia, the damping matrix, the stiffness matrix, which takes also into account the shear effect, and the gyroscopic matrix, can be defined by means of standard Lagrange's methods for beam elements as shown e.g. in [13], while the assembly of the total system (rotor, bearings and supporting structure) equations can be done by following the method described in [14]:
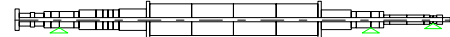
$$[\mathbf{M}]\ddot{\mathbf{x}} + [\mathbf{C}]\dot{\mathbf{x}} + [\mathbf{K}]\mathbf{x} = \mathbf{F}(\mathbf{x},t) \quad (24)$$

where $[\mathbf{M}]$ is the mass matrix, $[\mathbf{C}]$ is the complete damping matrix which includes also the gyroscopic matrix calculated at the operating speed, $[\mathbf{K}]$ is the stiffness matrix.

The modal analysis of the generator alone, performed at the operating speed of 3000 rpm, shows that it has three eigenfrequencies below 50 Hz, namely 13.07, 39.03 and 43.62 Hz. The corresponding modes are shown in figure 3-figure 5 (stiffness diameters are used for the rotor sketch).

It is worthy to note that the generator has also two other modes over 50 Hz, which could be excited by the UMP, whose eigenfrequencies are 83.22 (figure 6) and 100.4 Hz (figure 7). Anyhow the modal deformation at about 100 Hz is very reduced in the generator slotted part, therefore a 2X excitation due to UMP, being applied on this rotor part, would not be very effective on the system response.
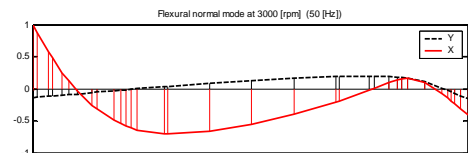
Figure 3: Normal mode at 13.07 Hz.

5 Copyright © 2005 by ASME

Eigenmode no. 2, ω = 2341.802 [rpm] (39.03003 [Hz]), ξ = 0.05784058

RAFT© 2.0
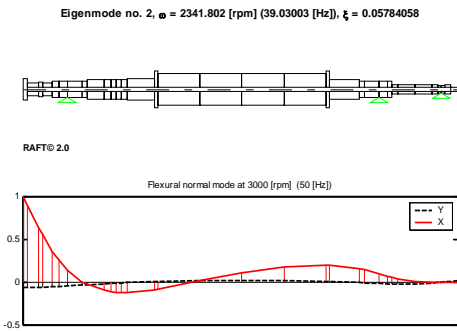
Figure 4: Normal mode at 39.03 Hz.

Eigenmode no. 3, ω = 2617.432 [rpm] (43.62387 [Hz]), ξ = 0.04566123

RAFT© 2.0
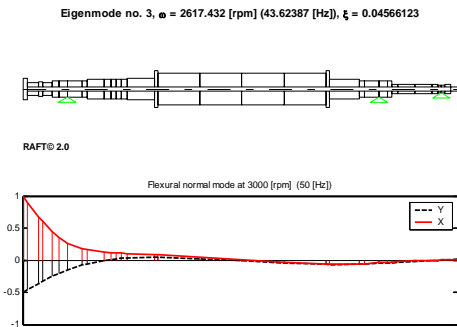
Figure 5: Normal mode at 43.62 Hz.

Eigenmode no. 4, ω = 4993.104 [rpm] (83.2184 [Hz]), ξ = 0.03549644

RAFT© 2.0
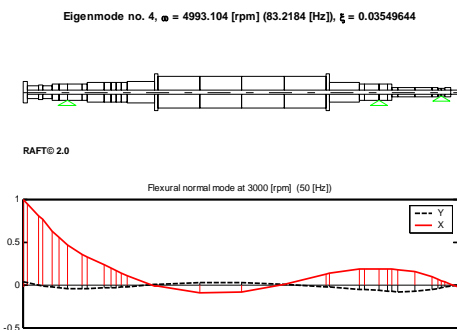
Figure 6: Normal mode at 83.22 Hz.

Eigenmode no. 5, ω = 6024.529 [rpm] (100.4088 [Hz]), ξ = 0.06525368

RAFT© 2.0
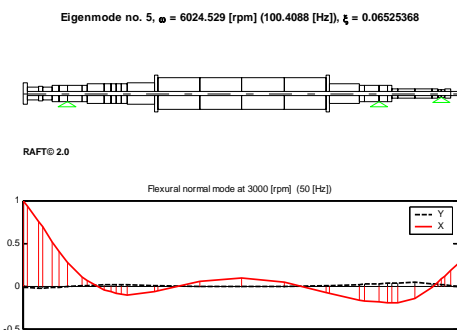
Figure 7: Normal mode at 100.4 Hz.

The external force vector $\mathbf{F}(\mathbf{x},t)$ of eq. (24) includes the original unbalance of the rotor and the effect of the UMP, therefore is not only function of time, but also of the vibration itself $\mathbf{x}$. In fact, the actual air-gap distribution depends on the relative position between the stator and the rotor as shown in

eqs. (14) and (15). Moreover, the UMP, acting on a rotor element, is applied into the first node of the element. The general j-th rotor element d.o.f.s (figure 8) are ordered as:

$$\mathbf{x}^{(j)} = \left\{ x_j \quad \vartheta_{x_j} \quad y_j \quad \vartheta_{y_j} \quad x_{j+1} \quad \vartheta_{x_{j+1}} \quad y_{j+1} \quad \vartheta_{y_{j+1}} \right\}^{\mathrm{T}} \quad (25)$$
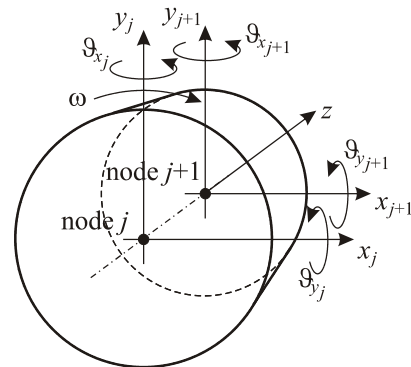

Figure 8: Reference systems of a general rotor element.

Then, if for simplicity the node of application of the unbalance does not correspond to any node of application of UMP, the structure of the column vector $\mathbf{F}(\mathbf{x},t)$ is typically:

$$\mathbf{F}(\mathbf{x},t) = \left\{ \begin{array}{l} 0 \quad \vdots \quad \underbrace{m\,e\,\omega^2\cos\omega t \quad 0 \quad m\,e\,\omega^2\sin\omega t \quad 0}_{\text{rotor node in which the unbalance is applied}} \quad \vdots \\ \vdots \quad \underbrace{F_{x,UMP}^{(k)} \quad 0 \quad F_{y,UMP}^{(k)} \quad 0}_{\substack{\text{first node of an element in which}\\ \text{the UMP is applied}}} \quad \vdots \quad 0 \quad \underbrace{0 \quad \cdots \quad 0}_{\text{foundation d.o.f.s}} \end{array} \right\}^{\mathrm{T}} \quad (26)$$

Since dynamic effects are considered, the effect of the weight is neglected. The non-linear system of equations in eq. (24) is integrated using the Newmark implicit method, in which the forcing vector of eq. (26) is recalculated at each time step: the UMP forces are calculated using eqs. (22) and (23) considering the air-gap distribution due to the vibration at the previous time step.

In other terms, in a general time step i-th, the generalized displacements, accelerations and velocities are:

$$\mathbf{x}_i = \left[\frac{1}{a\,\Delta t^2}[\mathbf{M}] + \frac{b}{a\,\Delta t}[\mathbf{C}] + [\mathbf{K}] \right]^{-1} \cdot$$

$$\cdot \left(\begin{array}{l} \mathbf{F}_{i-1}(\mathbf{x}_{i-1},t_i) + \left[\frac{1}{a\,\Delta t^2}[\mathbf{M}] + \frac{b}{a\,\Delta t}[\mathbf{C}] \right]\mathbf{x}_{i-1} + \\ + \left[\frac{1}{a\,\Delta t}[\mathbf{M}] - \left(1-\frac{b}{a}\right)[\mathbf{C}] \right]\dot{\mathbf{x}}_{i-1} + \\ + \left[\frac{1}{a}\left(\frac{1}{2}-a\right)[\mathbf{M}] - \Delta t\left(1-\frac{b}{2a}\right)[\mathbf{C}] \right]\ddot{\mathbf{x}}_{i-1} \end{array} \right) \quad (27)$$

6   Copyright © 2005 by ASME

Downloaded From: https://proceedings.asmedigitalcollection.asme.org on 06/29/2019 Terms of Use: http://www.asme.org/about-asme/terms-of-use

$$\ddot{\mathbf{x}}_i = \frac{1}{a\,\Delta t^2}\left(\mathbf{x}_i - \mathbf{x}_{i-1} - \dot{\mathbf{x}}_{i-1}\Delta t\right) - \frac{1}{a}\left(\frac{1}{2} - a\right)\ddot{\mathbf{x}}_{i-1} \qquad (28)$$

$$\dot{\mathbf{x}}_i = \frac{b}{a\,\Delta t}\left(\mathbf{x}_i - \mathbf{x}_{i-1}\right) + \left(1 - \frac{b}{a}\right)\dot{\mathbf{x}}_{i-1} + \Delta t\left(1 - \frac{b}{2a}\right)\ddot{\mathbf{x}}_{i-1} \qquad (29)$$

in which the part of the force vector $\mathbf{F}(\mathbf{x}_{i-1}, t_i)$ due to the UMP on an element is calculated using the air-gap distribution due to the position of the rotor element w.r.t. the stator at the time step $(i\text{-}1)$-th.

The constants a and b of the Newmark method are assumed respectively equal to 0.25 and 0.5, which is equivalent to the "trapezium rule" and assures that the implicit integration is unconditionally stable, without adding numerical damping (high values of b). In fact it can be proven that Newmark method is unconditionally stable if $b \geq 0.5$ and $a \geq 0.25(0.5 + b)^2$.

NUMERICAL RESULTS

The methods presented in the previous chapters have been applied to the considered model of the generator. Only the central part of the generator, that corresponding to the slotted part, namely elements 16, 17, 18 and 19, is relevant for the calculation of the UMP forces (figure 9). The diameter of these elements is 1024 mm.
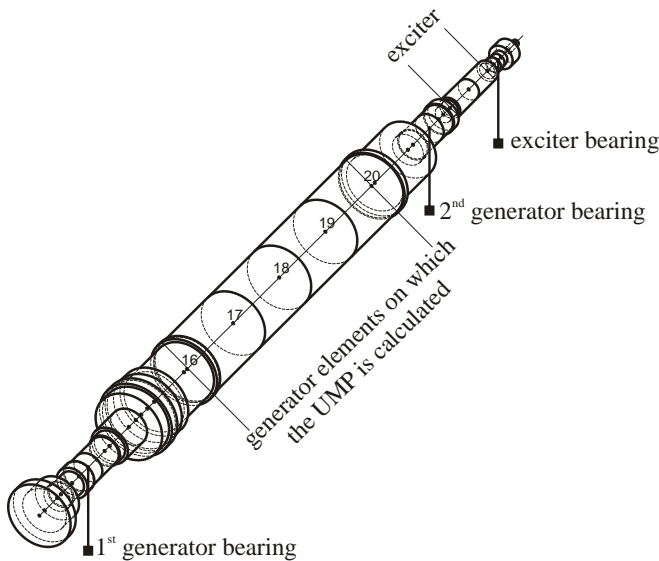

Figure 9: Generator elements on which the UMP is calculated.

For generators of this size, the nominal air-gap is generally 60 mm. Taking into account that the magnetic flux density B_r is limited to 1 T to avoid saturation occurrence in the iron core, this implies from eq. (20) that the magnetomotive force per each pole $\overline{M}_1/2$ is about 47746 A. If we consider seven coils per pole, each with a square section of 40×40 mm^2, the current density is 4.26 A/mm^2 that is rather acceptable.

Moreover, it should also be considered that in these machines, due to the presence of the anisotropy of the oil-film bearings, the centreline position is affected significantly by the geometry of the oil-film inside the bearing. Even without considering any other external forcing system, except oil-film forces and the weight, the journal assumes an attitude angle and is eccentric w.r.t. to the bearing case. This phenomenon is conceptually similar to the static eccentricity [1] [15]. Therefore the rotor is considered to have an eccentric offset of 50 μm in horizontal positive direction and 200 μm in vertical positive direction. These "offsets" are algebraically summed to the vibrations of the nodes in order to calculate the absolute vibrations w.r.t the stator and then the air-gap distribution and the UMP. Finally, an unbalance, simulating the residual unbalance of the machine, with amplitude of 1 kgm was applied on node 17.

The simulation presented here lasts 5 s and the time step Δt is assumed to be 1e−5 s. For the sake of brevity only some orbits of the nodes of the generator are show. In particular, the orbits of the nodes corresponding to the bearings are considered to be more significant, since on the real machines vibration measuring planes usually corresponds to the bearing positions, and are shown in figure 10-figure 12. Moreover also the orbit of a node in the slotted part (node 18) of the rotor is shown in figure 13. Note that the vibrations, and the orbits too, are referred to the centreline of the shaft, i.e. they do not consider the offset.
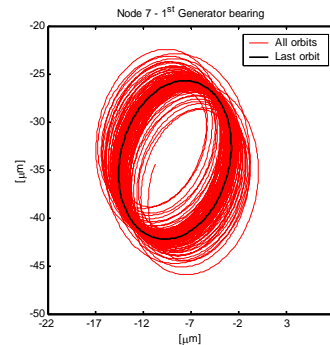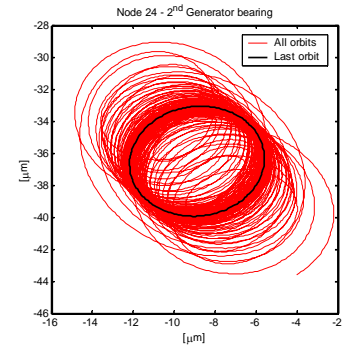

Figure 10: Rotor orbits in brg. #1.

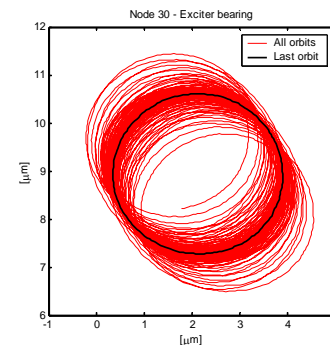**Figure 11**: Rotor orbits in brg. #2.
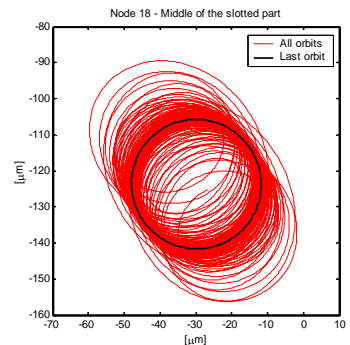

Figure 12: Rotor orbits in brg. #3.

Figure 13: Rotor orbits in the middle of the slotted part.

The orbits, shown in figure 10-figure 13, are rather elliptical in the generator bearings, while are practically circular in the middle part of the generator. Moreover they are not fixed

7   Copyright © 2005 by ASME

in the space but evolve around an average position, which is practically an attractor. A superficial analysis of the orbits could suggest that horizontal and vertical vibrations have only synchronous harmonic component in their spectra, but this opinion should be corrected once vibration spectra are considered.

The spectra in figure 14-figure 17, namely those of the vibrations in the bearings and in the middle of the generator slotted part, show the synchronous component (50 Hz) as the main one and also the presence of a 2X component at 100 Hz. Anyhow, 2X harmonic component is very small w.r.t. to 1X component, and this confirms the observation made in the previous chapter about the mode at about 100 Hz.

However also a super-synchronous component at 71.6 Hz is evident and a rich sub-harmonic spectrum is present with the higher component at 21.6 Hz, which is greater than the 2X component. The last fact indicates high energetic content in sub-synchronous vibration that explains the dynamical behaviour of the system around the attractor shown in figure 10-figure 13. Moreover, the presence of sub- and super-synchronous components, which are not integer multiple of the rotating speed, indicates that the UMP introduces non-linearities in the system behaviour.
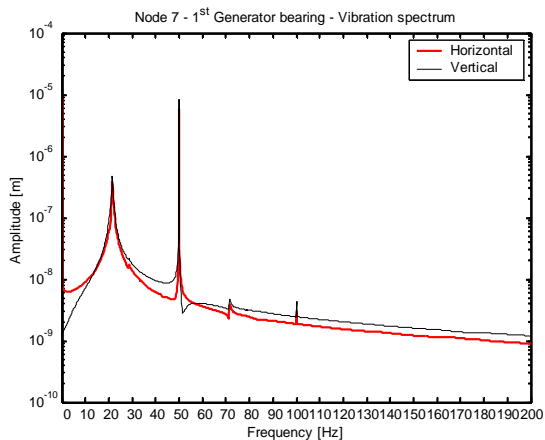

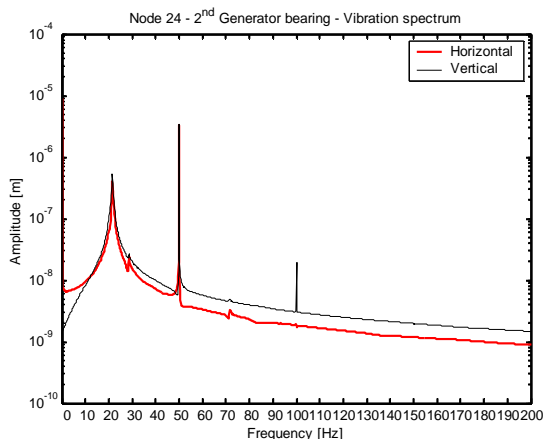**Figure 14**: Vibration spectrum in brg. #1.

Figure 15: Vibration spectrum in brg. #2.

The presence of non-linearites is confirmed also by the analysis of the UMP spectra, shown in figure 18-figure 21. Besides the presence of 1X and 2X harmonic components, the super-harmonic component at 71.6 Hz is more evident than in the vibration spectra. In regards to the sub-harmonic

components, once again the spectra are very rich and two components are evident: the highest at 21.6 Hz and a secondary one at 28.6 Hz.
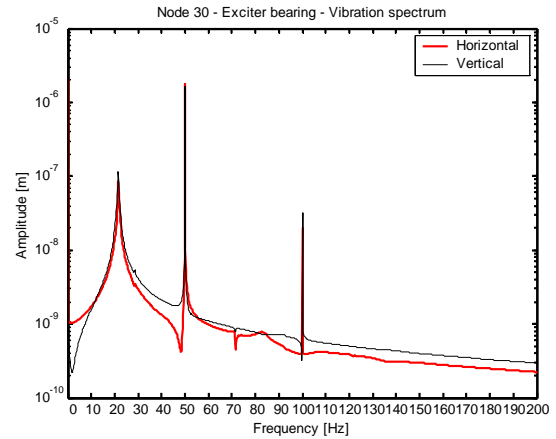

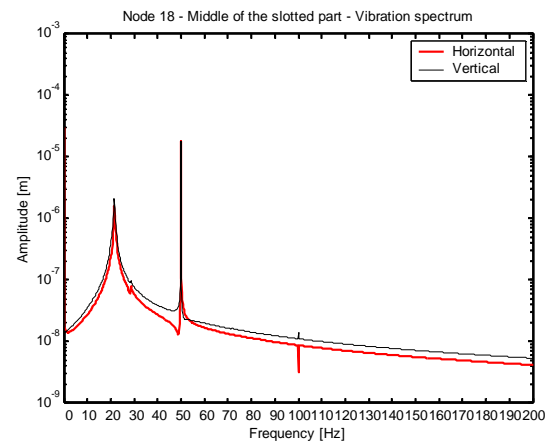**Figure 16**: Vibration spectrum in brg. #3.

Figure 17: Vibration spectrum in the middle of the slotted part.

Note that traditional models dealing with UMP in generators, like [1] [2], do not allow emphasizing the presence of 1X force component, nor the presence on non-linearity.

Table 2 shows the magnitude of UMP forces. It is interesting to note that the total of the static pull force is about 33431 N that can be compared with the weight of the generator equal to 519781 N. The other harmonic components can be compared with the unbalance, which is 98596 N. Moreover, the sub-synchronous component at 21.6 Hz is sensibly greater than the 2X component, underlying the relevance of non-linear effects in the UMP phenomenon.

The last confirmation of the presence of non-linear effects in the UMP is made by simulating the dynamical behaviour of the considered generator without the presence of the magnetic pull. The Newmark method is used again and in the eq. (26), which represents the excitation force, the only terms different from zero are those corresponding to the unbalance. Similarly, the simulation lasts 5 s and the time step Δt is assumed to be 1e–5 s.

Figure 22 shows the orbit in bearing #1 that can be compared with figure 10. Also in this case the vibrations are referred to the centreline. The orbit shape is comparable even if

8   Copyright © 2005 by ASME

the amplitude is little minor, but in this case the orbits are precisely superposed. The comparison between the last 1X filtered orbits of the cases, using the SDI (Shape and Directivity Index [16] [17]), is shown in table 3.

Table 2: UMP force magnitudes.

	Static force[(1)] [N]	Static resultant[(1)] [N]	1X (50 Hz) [N]	2X (100 Hz) [N]	Super sync. (71.6 Hz) [N]	Sub sync. (21.6 Hz) [N]
$F_{x,UMP}^{(16)}$	−1837.39	8101.52@ −103.11°	5284.41	28.21	4.36	158.33
$F_{y,UMP}^{(16)}$	−7890.42		5404.68	60.85	4.33	219.63
$F_{x,UMP}^{(17)}$	−1788.95	7569.03@ −103.67°	3163.64	10.00	2.80	160.65
$F_{y,UMP}^{(17)}$	−7354.58		3220.70	22.21	2.89	223.77
$F_{x,UMP}^{(18)}$	−1918.17	8087.21@ −103.72°	1847.05	3.37	1.89	152.29
$F_{y,UMP}^{(18)}$	−7856.44		1857.45	7.98	2.09	212.32
$F_{x,UMP}^{(19)}$	−2245.28	9674.15@ −103.42°	970.18	0.74	1.36	133.24
$F_{y,UMP}^{(19)}$	−9409.99		950.09	2.04	1.64	185.41

[(1)] Static force component in *x* and *y* direction and resultant are referred to the reference system *S* of figure 1.
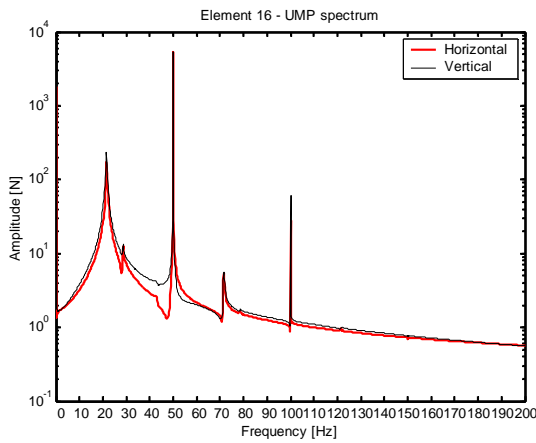

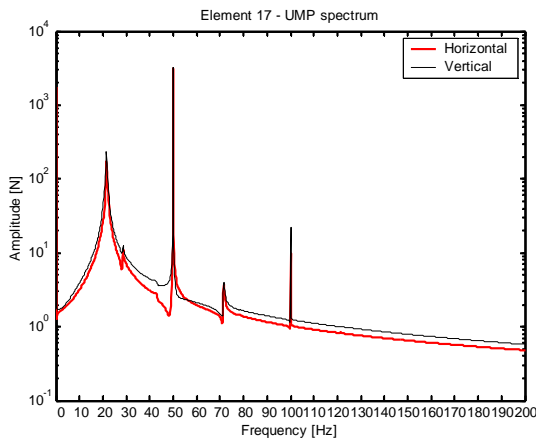**Figure 18**: UMP spectrum on element 16.

Figure 19: UMP spectrum on element 17.

Moreover, the centre of the orbit corresponds to the centreline, contrarily to the previous case. The absence of non-linearities in this case is confirmed by the vibration

spectrum, shown in figure 23 for the same bearing. The synchronous component is the only one evident and no sub- or super-synchronous are present. Similar results are obtained for the other generator nodes.
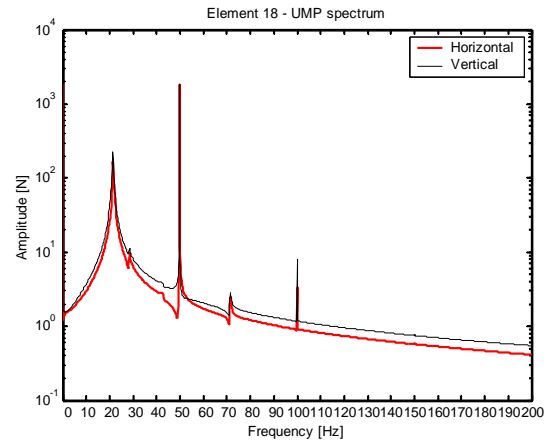

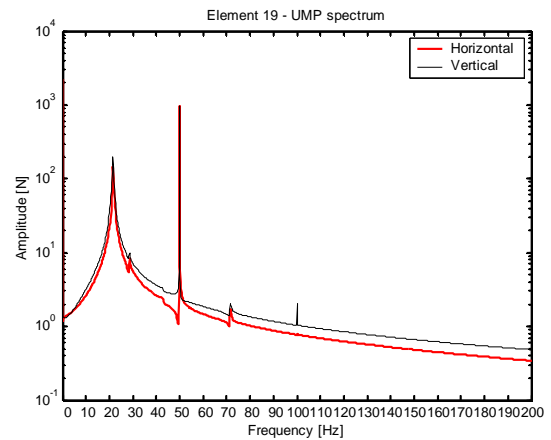**Figure 20**: UMP spectrum on element 18.

Figure 21: UMP spectrum on element 19.

Table 3: Comparison of the generator 1X filtered orbits w/ and w/o UMP.

	SDI	Major axis amplitude [μm]	Major axis inclination [degrees]
W/ UMP	0.683	16.69	73.76°
W/o UMP	0.681	14.05	74.07°

CONCLUSIONS

The phenomenon of the Unbalanced Magnetic Pull represents one of the most interesting cases in the electrical power generation machines that require a modelling both from the mechanical and electric point of view. In the present paper, a rather sophisticated model is introduced to calculate the magnetic pull in generators, which starts from the exact determination of the distribution of the air-gap and then defines, by means of Maxwell stress calculation, the static and dynamic forces that are caused by the asymmetric distribution

9   Copyright © 2005 by ASME

of the air-gap. An application is introduced on a smooth generator of 320 MW turbo-generator, operating at 3000 rpm, whose dynamic behaviour is simulated in the time domain. The obtained results show that the magnetic pull in generators, besides the static component, has 2X harmonic component, as it is also obtained by simplified models, but it has also synchronous harmonic component and sub- and super-synchronous components, which indicate the non-linearity of this kind of excitation in the dynamic behaviour of the rotor.
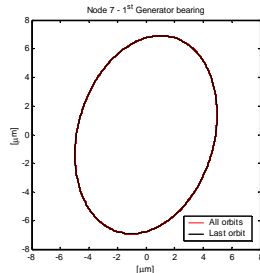

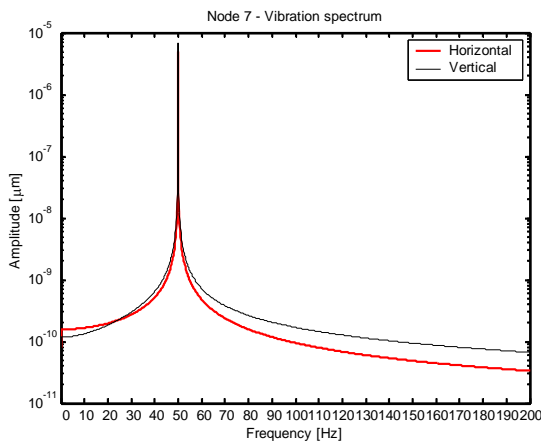
Figure 22: Rotor orbits in brg. #1 due to unbalance only.

Figure 23: Vibration spectrum in brg. #1 due to unbalance only.

REFERENCES

[1] Stoll RL, "Simple computational model for calculation the unbalanced magnetic pull on a two-pole turbogenerator rotor due to eccentricity", IEE Proc.-Electr. Power Appl., 144(4), July 1997, 263-270.

[2] Guo D, Chu F and Chen D, "The Unbalanced Magnetic Pull and its Effects on Vibration in a Three-Phase Generator with Eccentric Rotor", Journal of sound and Vibration, 254(2), 2002, 297-312.

[3] Dorrel DG, "Calculation of Unbalanced Magnetic Pull in Small Cage Induction Motors with Skewed Rotors and Dynamic Rotor Eccentricity", IEEE Transactions on Energy Conversion, 11(3), Sept 1996, 483-488.

[4] Gustavsson RK and Aidanpää J-O, "The influence of Magnetic Pull on the Stability of Generator Rotors", paper ISROMAC10-2004-101, Proc. of The 10th Intl. Symposium on Transport Phenomena and Dynamics of Rotating Machinery, Honolulu, Hawaii, March 7-11, 2004, 1-9.

[5] Smith AC and Dorrel DG, "Calculation and measurement of unbalanced magnetic pull in cage induction motors with eccentric rotors. Part 1: Analytic model", IEE Proc.-Electr. Power Appl., 143(3), May 1996, 193-201.

[6] Dorrel DG, Thomson WT and Roach S, "Analysis of Airgap Flux, Current, and Vibration Signals as a Function of the Combination of Static and Dynamic Airgap Eccentricity in 3-Phase Induction Motors", IEEE Transactions on Industry Applications, 33(1), Jan/Feb 1997, 24-34.

[7] Dorrel DG, "Experimental Behaviour of Unbalanced Magnetic Pull in 3-Phase Induction Motors with Eccentric Rotors and the Relationship with Tooth Saturation", IEEE Transactions on Energy Conversion, 14(3), Sept 1999, 304-309.

[8] Binns KJ and Dye M, "Identification of principal factors causing unbalanced magnetic pull in cage induction motor", Proc. IEE, 120, 1973, 349-354.

[9] Bachschmid N and Diana G, "Reduction of twice per revolution vibration levels due to weight effect in large turbogenerators", Proc. of IMechE Second International Conference Vibration in Rotating Machinery, Churchill College, Cambridge, 2-4 Sept 1980, 203-208.

[10] Bachschmid N and Frigeri C, "Some results on the twice-per-revolution balancing of generators", Proc. of IFToMM International Conference Rotordynamic Problems in Power Plants, Rome, 28 Sept- 1 Oct 1982, 49-54.

[11] Bachschmid N and Pennacchi P, "Subtask 4.6 – Polar Stiffness Asymmetry Model", Brite EuRam Project No BE95-2015 "MODIAROT", Contract No BRPR-CT95-0022, 1999, pp. 1-7.

[12] Someya T., Journal-Bearing Databook, Springer-Verlag, 1989.

[13] Lalanne M. and Ferraris G., Rotordynamics Prediction in Engineering, John Wiley & Sons Inc, Chichester, England, 1998.

[14] Pennacchi P, Bachschmid N, Vania A, Zanetta GA and Gregori L, "Use of Modal Representation for the Supporting Structure in Model Based Fault Identification of Large Rotating Machinery: Part 1 – Theoretical Remarks", in press on Mechanical Systems and Signal Processing, available on-line on ScienceDirect.

[15] Frosini L and Pennacchi P, "Detection and modelling of rotor eccentricity in electrical machines: an overview", IMechE paper C623/060/2004, Proc. of 8th International Conference on Vibrations in Rotating Machinery, 7-9 September 2004, Swansea, Wales, ISSN 1356-1448, ISBN 1-86058-447-0, 501-510.

[16] Lee CW and Han Y-S, "The Directional Wigner Distribution and its Applications", Journal of Sound and Vibration, 216(4), 1998, 585-600.

[17] Pennacchi P and Vania A, "Diagnosis and model based identification of a coupling misalignment", in press on Shock and Vibration, 1-20.